Heliyon 9 (2023) e12854

Contents lists available at ScienceDirect

Heliyon

journal homepage: www.cell.com/heliyon

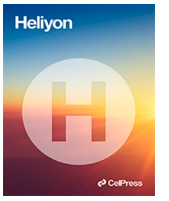

Research article

Development of ceramic grade red iron oxide pigment from waste iron source

Juliya Khanam [a,*], Md. Rashib Hasan [b], Bristy Biswas [a], Shirin Akter Jahan [a], Nahid Sharmin [a], Samina Ahmed [a], Sharif Md. Al-Reza [b]

[a] *Institute of Glass and Ceramic Research and Testing (IGCRT), Bangladesh Council of Scientific and Industrial Research (BCSIR), Dhaka, 1205, Bangladesh*

[b] *Department of Applied Chemistry and Chemical Engineering, Islamic University, Kushtia, Bangladesh*

ARTICLE INFO

Keywords:
Hematite
Nanoparticle
Recycling
Morphology

ABSTRACT

Ceramic grade red iron oxide (α-Fe_2O_3) nanoparticles pigments have been synthesized from waste condensed milk containers which contain a prominent amount of iron (93.2%). The synthesis method comprised of two steps: in the first step ferrous sulfate was prepared following an acid leaching method; while the second step was oxidation and calcination of ferrous sulfate to produce desired α-Fe_2O_3 in nano form. The structure, functional groups, chemical state, morphology, particle size, surface area, elemental, thermal analysis and magnetic properties of the samples were investigated using XRD, FTIR, XPS, SEM, BET, EDS, TG-DT and VSM respectively. Pure hematite (α-Fe_2O_3) phase was confirmed by XRD and the average crystal sizes were in the range 34–126 nm have been performed by Debye-Scherer's formula, which are consistent with the results as achieved from SEM images. Agglomerated irregular spherical nanoparticles (45–149 nm) were found in SEM image. The surface chemistry and the chemical state (Fe^{3+}) of the hematite nanoparticles was also confirmed by XPS. The mesoporous nature of the nanoparticles with high surface area were measured by BET and it has been revealed that the BET specific surface area (33.55 m^2/g) was marginally higher than the commercial one. The magnetic nature of the nanoparticles was portrayed by VSM and the nanoparticles showed the ferromagnetic behavior. Moreover, particle size distributions and zeta potential values have been also measured by DLS.

1. Introduction

Nanomaterials based on iron oxide have attracted a global deal of research interest due to their unique superior properties, easy availability, low cost, environmental compatibility, high performance and non-toxicity that diverge greatly from their bulk materials [1-4]. Among different metal oxide materials iron oxide is an important transition metal oxide and sixteen different types of iron oxides are known to date [4,5]. Magnetite (Fe_3O_4), maghemite (γ-Fe_2O_3) and hematite (α-Fe_2O_3) are three of the most commonly phases in nature and they play a wide range of important applications such as catalysis, microwave absorption, gas sensor, solar cell, electrochemistry, magnetization, biomedical science, pigment, environmental applications and so on [4-11]. Among the iron oxides hematite (α-Fe_2O_3) is chemically and thermodynamically more stable polymorph in ambient conditions [10,12–14]. Hematite (α-Fe_2O_3) has a

* Corresponding author. ;
E-mail addresses: juliyakhanom@gmail.com, juliyakhanom@bcsir.gov.bd (J. Khanam).

https://doi.org/10.1016/j.heliyon.2023.e12854
Received 19 July 2022; Received in revised form 25 December 2022; Accepted 4 January 2023
Available online 9 January 2023

corundum type crystal structure [15] and it has attracted extensive interests in commercial and industrial application as a pigment, catalyst, gas sensor, rechargeable lithium ion batteries [16], photo anode, nano-fluid, magnetic fluid [17], construction material [18], electrode materials owing to its low cost, high resistance to corrosion and environment friendly properties [19]. Different methods for synthesis of hematite nanoparticles were described in the literature including solvothermal process, hydrothermal approach, co-precipitation method, sol-gel method, ultrasonic irradiation, hydrolysis method, micro-emulsion method, sonochemical synthesis [20,21], combustion, solvent evaporation, mechanical millings [22], reverse micelles [23], high energy ball milling, spray pyrolysis [24], green synthesis [25,26], calcination etc. Different methods have some advantages and disadvantages. The green approach to nanoparticle synthesis being a cheap method and there is no requirement for high pressure, energy, temperature or toxic chemicals. In our present study, an attempt of finding out easy and cost effective way has been aimed to prepare hematite nanoparticles from waste condensed milk containers which contain more than 90% iron in it. No special instrument is needed in our synthesis method as well as no toxic chemicals are used. Environmental problem is a great concern nowadays. Natural sources of everything are decreasing [27] as well as ores of different types of minerals are also decreasing day by day [28]. Recycling of waste products may be a helpful way to reduce our dependence on natural sources [29]. Recycling is considered to be a good practice as it has good chances to save environment through the saving of primary resources and reduction of the negative consequences on environment resulting from landfill [30]. At present, waste materials containing higher iron percentage (≈72% Fe), are produced in massive volumes which is approximately five million tons worldwide [31]. Some iron enriched waste materials carry a handy amount of heavy metals like Hg, As, Cd and if left unused may have serious impact on environment mainly on soil and water. Therefore, the easy disposal of these wastes is not a suitable option if disposal cost and soil pollution are taken into account. Thus, it should be taken as an urgency to recover and recycle useable materials to get over the waste disposal issues [32-34].

Finding out easy and cost effective way to reuse waste products may be a handy way to save primary natural sources. Recycling of iron containing wastes produced from different types of industries is really a hot topic [35]. Recycling of these wastes is very helpful in controlling environmental pollution and also ensure their reutilization [9]. For a developing country like Bangladesh, it means a lot. A huge amount of iron containing recyclable product produced from steel industry, rerolling mills, vehicle components, huge amount of containers made from iron are being wasted due to the enough lack of scientific knowledge. As time goes on, they get rusted. Though this type of product is considered as a waste material, it can be used as an important raw material for the synthesis of iron oxide [36-38]. So in the present work, we focus on the synthesis of hematite (α-Fe_2O_3) nanoparticles from waste condensed milk container by simple acid leaching followed by crystallization to produce ferrous sulfate and then calcined it by adding suitable oxidizing agent. The synthesized hematite (α-Fe_2O_3) nanoparticles were characterized by XRD, XPS, FTIR, BET, SEM, DLS, TG-DT and VSM.

2. Methodology

2.1. Materials and reagents

In this study locally procured and analytical grade reagents were used. Sulfuric acid, H_2SO_4 (Merck, Germany) and Sodium nitrate, $NaNO_3$ (Merck Germany) were used for the preparation of pigment grade red iron oxide The waste condensed milk containers were used as a raw material for preparation of ferrous sulfate were collected from local market (tea stall) of Bangladesh. Chemical compositions of collected raw materials were investigated by using Wavelength Dispersive X-ray Fluorescence, WDXRF (Model no: Rigaku ZSX primus IV). Chemical composition of the milk container is given in Table 1.

2.2. Preparation of ferrous sulfate

Before synthesis of hematite we had to synthesis ferrous sulfate from waste condensed milk container as a starting material for synthesis of hematite. In the present study ferrous sulfate and hematite were prepared in two steps: in the first step ferrous sulfate was prepared following an acid leaching method; while the second step was oxidation and calcination of ferrous sulfate to produce desired α-Fe_2O_3 in nano form. Prior to the synthesis procedure the collected cans were thoroughly washed, cleaned and chopped into small pieces to ensure maximum leaching. However a requisite quantity of these chips were then taken in a closed vessel reactor containing 2.8 M H_2SO_4 The vessel temperature was 100 °C and the leaching reaction was continued for 4 h. After completing leaching period, the extracted liquor was separated and crystallized to get the pure product. A vacuum drier was used to dry the product [39]. The possible reaction for preparation of ferrous sulfate from condensed milk container is given below:

$$Fe + H_2SO4 \rightarrow FeSO_4.7H_2O + \uparrow H_2$$

$$Othermetal\ (Na, Mg, Al\ and\ so\ on) + SO_4 \rightarrow Metal\ Sulfate + \uparrow H_2$$

Table 1
Chemical composition of milk container.

Component	Na	Mg	Al	Si	P	S	Cl	K	Cr	Mn	Fe	Ni	Cu	Sn
Mass %	2.43	0.13	0.34	0.36	0.04	0.93	0.63	0.11	0.03	0.18	**93.2**	0.02	0.02	1.54

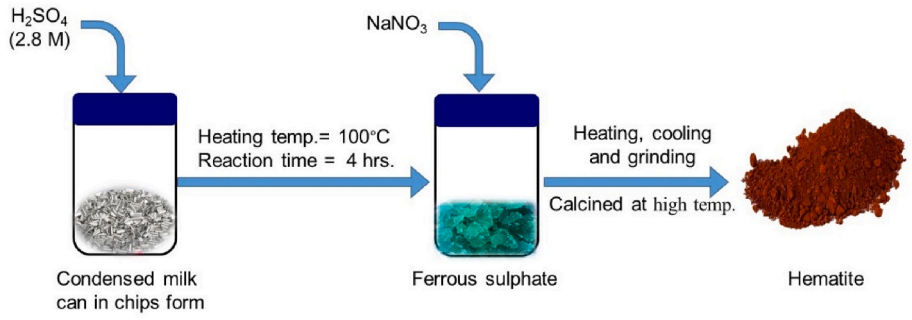

Fig. 1. Schematic diagram of synthesis α-Fe_2O_3 nanoparticles from waste condensed milk cans.

2.3. Synthesis of hematite

The synthesized hydrated ferrous sulfate crystal was then dried at 60 °C temperature for several hours to get monohydrated ferrous sulfate. Thereafter, a fixed amount of dried ferrous sulfate sample was taken in porcelain and mixed with suitable redox reagent (sodium nitrate). The ratio of $FeSO_4$ to $NaNO_3$ was maintained at 1:0.02. The mixture was then heated slowly at a burner for 2 h and then reheated vigorously for 30 min. After heating, cooling, and grinding, the mixture was calcined at 600 °C and 700 °C for 3 and 4 h each time as well as 6 h at 800 °C in a muffle furnace. The calcined samples were cooled, ground and washed several times to reduce the impurities and soluble component. Finally, the washed samples were filtered and then dried in an oven at 100 °C for one to 2 h. The obtained hematite was then again ground. The mechanism of formation of α-Fe_2O_3 nanoparticles from waste condensed milk cans is shown in Fig. 1.

2.4. Characterization

The crystal structure and the phase composition of the α-Fe_2O_3 have been examined by X-ray Diffractometer (Rigaku SmartLab SE) operating with a copper k-alpha ($\lambda = 1.5406$ Å) source and 0.02° step width, where the scan speed range was 50°/min radiation over a 2θ range of 10°–80°. FTIR spectrum between 4000 and 500 cm^{-1}have been recorded by Fourier transform Infrared Spectrometer (Model: Shimadzu Prestige 21). The surface morphology of α-Fe_2O_3 nanoparticles was carried out by using Scanning Electron Microscopy (MA15 VP-SEM, Carl Zeiss Evo, Uk). The chemical composition of the α-Fe_2O_3 nanoparticles was performed by Energy Dispersive Spectrometer (EDAX team, EDAX, USA) spectral analysis. An X-ray photoelectron spectrometer (K-alpha, Thermo Scientific, Czech Republic) was used to evaluate the chemical and oxidation state of the atoms in the sample compound by using a monochromatic source of Al K-alpha (1486.69 eV) X-ray source. Survey scan analyses of the samples were carried out with spot size area of 400 μm^2, pass energy of 200 eV, number of scan of 5, dwell time of 10 ms and energy step size of 1.0 eV. High resolution scan analyses of the samples were performed to obtain the spectra of Fe 2p. The pass energy for the high resolution scan analysis was 50 eV, dwell time 50 ms and the energy step size of 0.1 eV. The calibration of the binding energy curves were performed using C 1s peak at 284.8 eV. The N_2 adsorption-desorption isotherm curves were obtained at 77 K using a BET sorptometer (BET-201-A, PMI, USA, Software: Betwin). The samples were first outgassed at 120 °C for 5 h. BET specific surface area (S_{BET}, m^2/g) was calculated by the multi-point Brunauer-Emmet-Teller (BET) model from the adsorption data in relative pressure p/p_0 between 0.05 and 0.3, where p and p_0 are the equilibrium and saturation pressure of nitrogen respectively. Size distribution and polydispersity index (PDI) of the hematite nano particles dispersed in aqueous solution were accomplished through Dynamic Light Scattering method (DLS) using a Malvern Zetasizer Ultra (ZSU5700). Zeta potential measurements were also measured with a Malvern Zetasizer Ultra (ZSU5700) using the technique of Laser Doppler Velocimetry (LDV). The thermal response of the samples was studied with a combined TG-DTA analyzer (TG/DTA 6300). Thermal analysis was recorded at a scan rate of 20 °C/min in alumina crucible under a dynamic nitrogen atmosphere from 25 °C to 900 °C. The magnetic property of α-Fe_2O_3 nanoparticles was characterized by Lakeshore cryotronics 8400 series VSM at room temperature in an applied magnetic field sweeping from −15,000 to 15,000 Oe.

3. Result and discussion

3.1. Structural analysis by XRD

The positions of all the diffraction pattern of the samples coincide with the maxima characteristic of the hematite phase (JCPDS card 01-080-237, 04-01) were observed is shown in Fig. 2. No diffraction line corresponding to other phases has been observed, indicating high purity of the samples. The major XRD peaks at 24.14°, 33.24°, 35.61°, 40.81°, 49.47°, 54.09°, 57.62°, 62.46°, and 64.13° 2θ were assigned to the (0 1 2), (1 0 4), (1 1 0), (1 1 3), (0 2 4), (1 1 6), (0 1 8), (2 1 4) and (3 0 0) planes respectively. The percent purity of the synthesized α-Fe_2O_3 samples calcined at different conditions were also confirmed by Wavelength Dispersive X-ray Fluorescence, WDXRF (Model no: Rigaku ZSX primus IV) as shown in Table 2. The broad diffraction peaks (calcined at 600°C, 3 h) can be observed, as expected for monocrystalline particles [10] as shown in Fig. 2. By using Debye-Scherrer's formula (Eqn. (1)), the

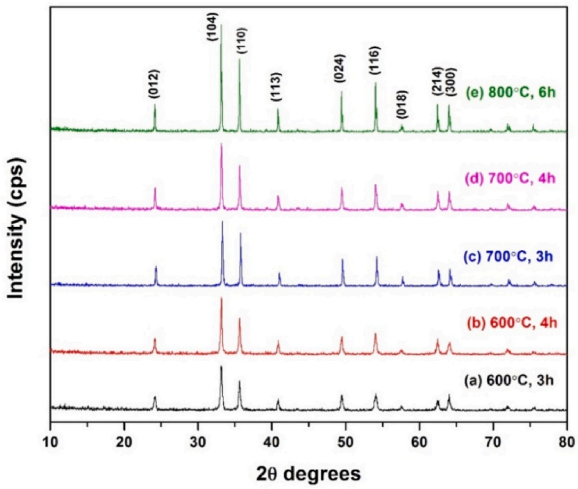

Fig. 2. X-ray diffraction pattern of α-Fe_2O_3 calcined at different temperatures and times.

average crystallite sizes 'D' have been calculated from the highest intensity peaks (104) for the nano particles synthesized at discrete condition and the results were also listed in Table 2.

$$D = \frac{k\lambda}{\beta \cos\theta} \tag{1}$$

where *K* refers to the shape factor (0.9), λ is the wavelength of CuKα = 1.5406 Å, β is the Full Width Half Maximum (FWHM) in Radians and θ is the diffraction angle. The lattice parameters (a = b, and c) have been calculated by the following expression [4], where d is the inter-reticular distance, a and c are the lattice parameters and h, k, l are the Miller indices (Eqn. (2)) and the results were listed in Table 2.

Table 2
Percent purity, crystallite size and lattice parameters of the synthesized α-Fe_2O_3 samples calcined at different conditions.

Calcination Temperature (°C) & Time (h)	Mass Percentage	Average Crystallite Size (nm)	Lattice Parameters	
			a (Å) = b (Å)	c (Å)
600, 3	98.4	34	5.03462	13.75789
600, 4	98.6	43	5.03551	13.74831
700, 3	99.6	83	5.02139	13.70550
700, 4	99.2	68	5.03563	13.75729
800, 6	99.3	126	5.03723	13.75045

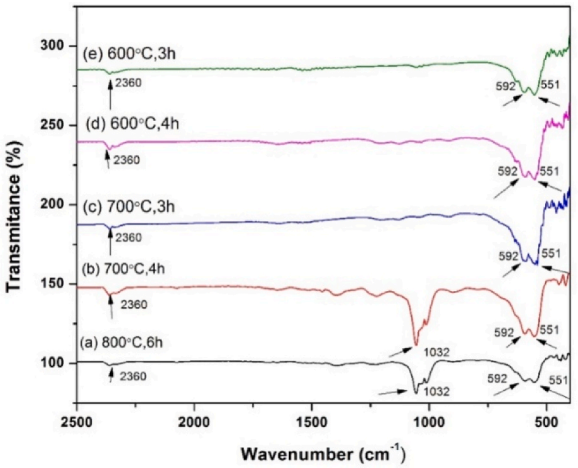

Fig. 3. FTIR pattern of α-Fe_2O_3calcinedat different temperatures and times.

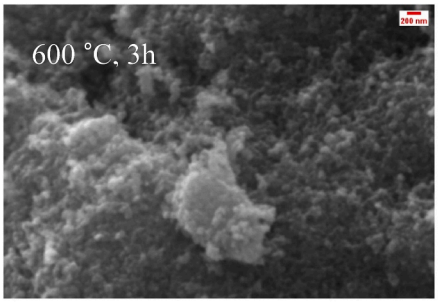

(a)

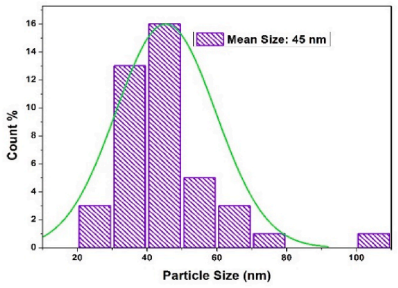

(a)

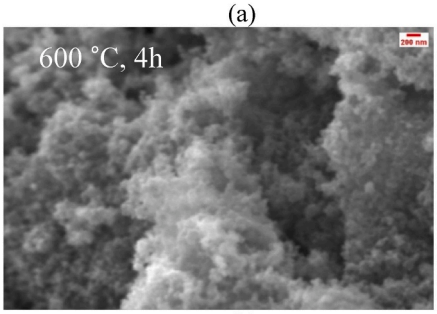

(b)

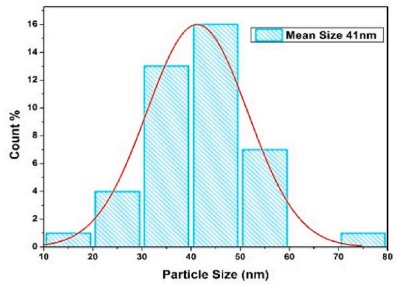

(b)

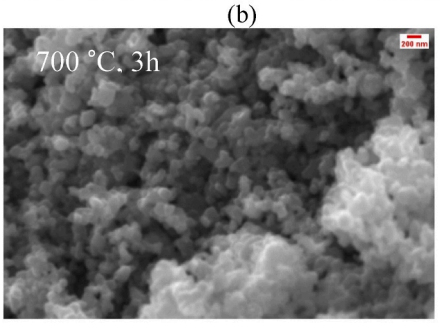

(c)

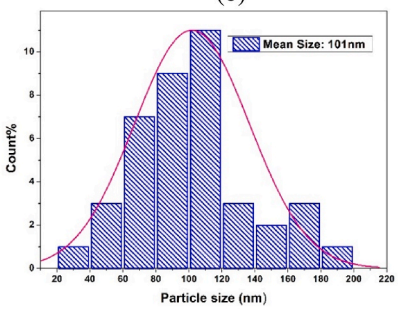

(c)

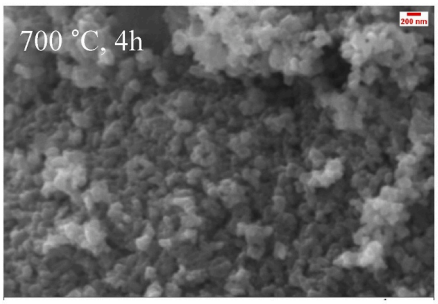

(d)

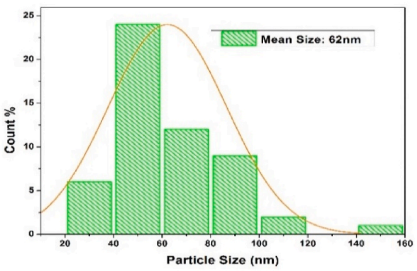

(d)

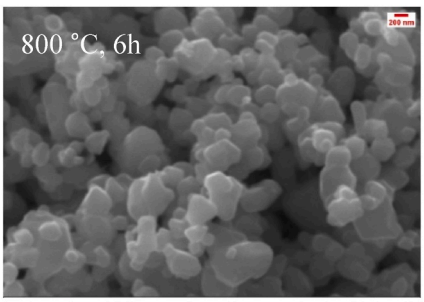

(e)

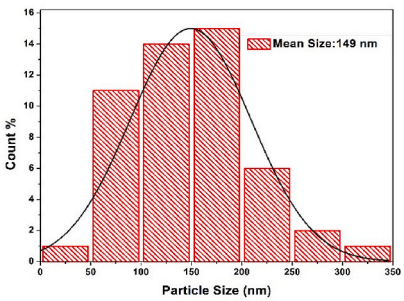

(e)

(caption on next page)

Fig. 4. SEM image and size distribution of α-Fe_2O_3 nanoparticles calcined at distinct temperatures and times (a) 600 °C, 3 h (b) 600 °C, 4 h (c) 700 °C, 3 h (d) 700 °C, 4 h (e) 800 °C, 6 h.

Table 3
SEM result of α-Fe_2O_3 nanoparticles calcined at different temperatures and times.

Calcination Temperature (°C) & Time (h)	Average Particle size (nm)
600, 3	45
600, 4	41
700, 3	101
700, 4	62
800, 6	149

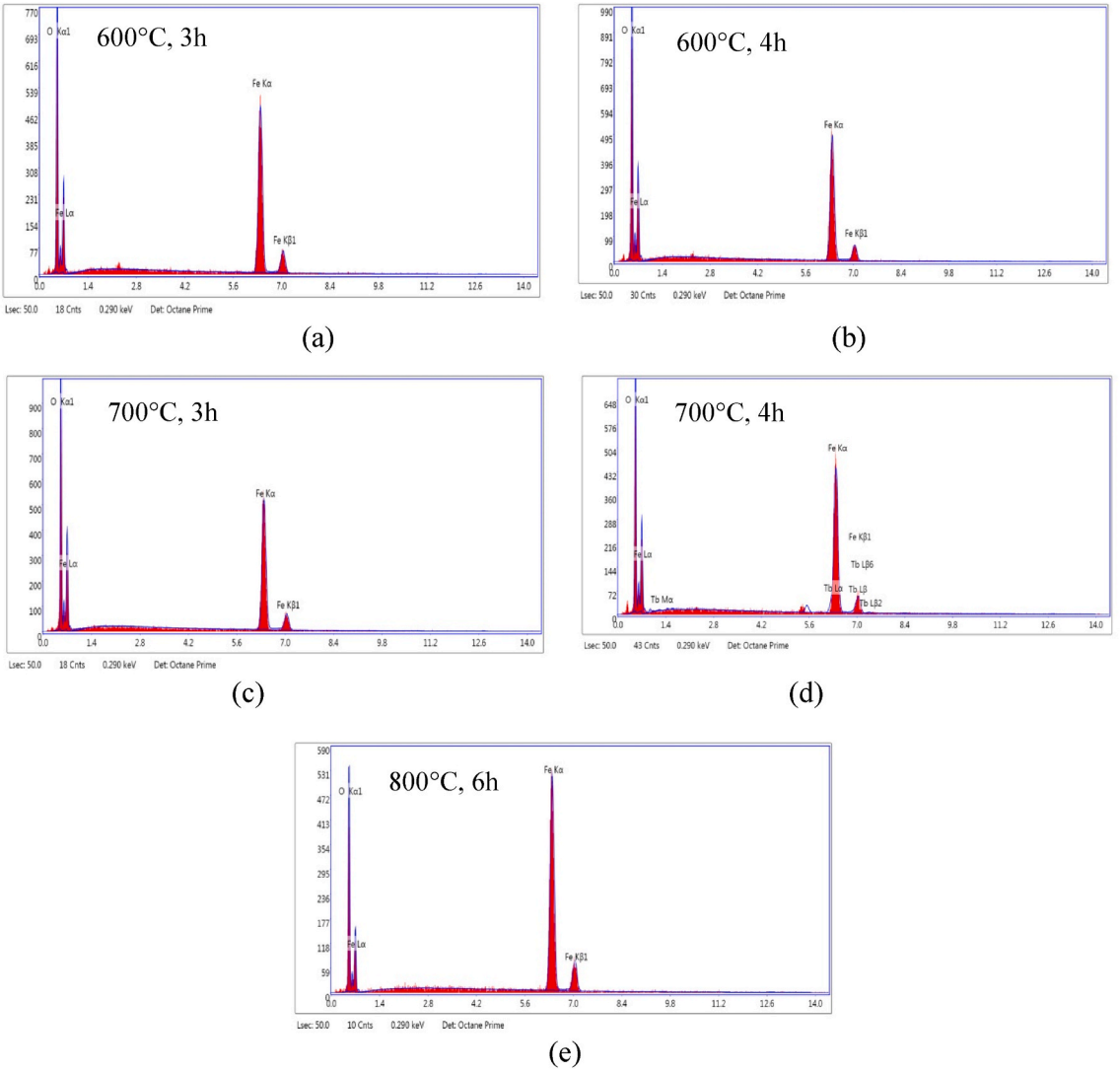

Fig. 5. EDS spectra of α-Fe_2O_3 nanoparticles calcined at different temperatures and times (a) 600 °C, 3 h (b) 600 °C, 4 h (c) 700 °C, 3 h (d) 700 °C, 4 h (e) 800 °C, 6 h.

Table 4
EDS result of α-Fe_2O_3 nanoparticles calcined at different temperatures and times.

Calcination Temperature (°C) & Time (h)	Atomic (%)		
	O	Fe	Fe/O
600, 3	56.77	43.23	0.76
600, 4	62.29	37.71	0.60
700, 3	61.06	38.94	0.63
700, 4	54.44	39.49	0.72
800, 6	44.72	55.28	1.23

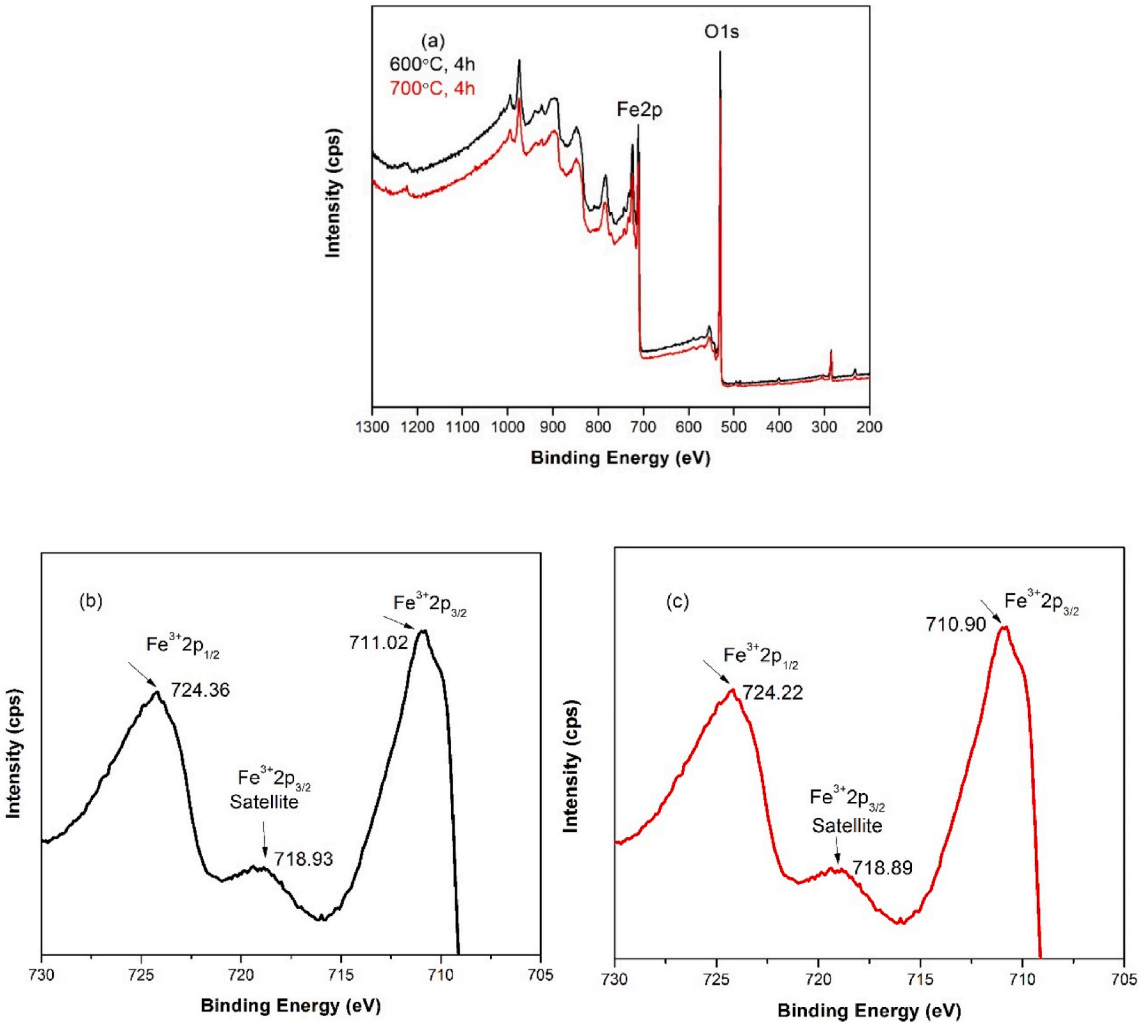

Fig. 6. XPS data of α-Fe_2O_3nanoparticles (a) survey spectrum data calcined at 600 °C, 4 h and 700 °C, 4 h (b) Fe 2p spectrum calcined at 600 °C, 4 h (c) Fe 2p spectrum calcined at 700 °C, 4 h.

$$d_{hkl} = \frac{1}{\sqrt{\frac{4}{3a^2}\left(h^2 + k^2 + l^2\right) \pm \frac{l^2}{c^2}}} \tag{2}$$

3.2. Functional group analysis by FTIR

Fig. 3 shows the FTIR spectra of α-Fe_2O_3 samples calcined at different conditions. The absorption bands positioned in the range of 450–500 $cm^{-1}$and 540–600 cm^{-1} are the representative absorption bands for the stretching Fe–O band [3,12,13,16,18]. The absorption band at 1032 cm^{-1} (sample calcined at 700 °C, 4 h and 800 °C, 6 h) also corresponds to Fe–O crystalline vibrations,

Table 5
The specific surface area, total pore volume and average pore diameter of the nanoparticles calcined at 600 °C, 4 h and 700 °C.

Calcination Temperature (°C) & Time (h)	Specific surface area (m^2/g)	Total Pore Volume (cm^3/g)	Average Pore Diameter (nm)
600, 4	33.55	0.1028	12.26
700, 4	12.74	0.0260	8.16

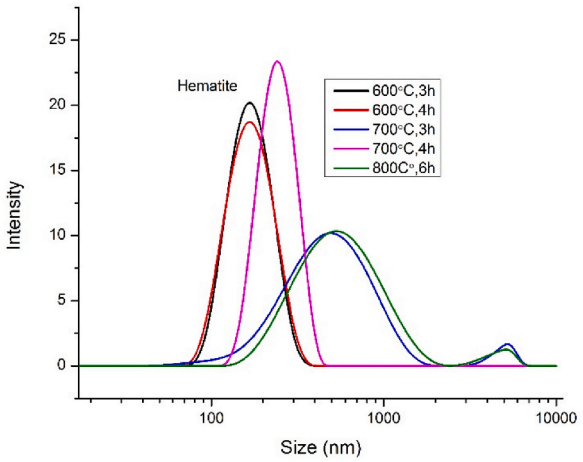

Fig. 7. Particle size distribution by dynamic light scattering method of α-Fe_2O_3nanoparticles calcined at different temperatures and times.

characteristic of α- Fe_2O_3, hence confirming hematite formation [25]. The weak adsorption band at 2360 cm^{-1} is an asymmetric stretching peak of CO_2 in the air [40].

3.3. Morphological analysis by SEM

Fig. 4(a–e) shows the SEM micrographs and particle size distribution histogram of α-Fe_2O_3 nanoparticles calcined at different temperatures and times. As shown in Fig. 4(a–e) irregular spherical shape nanoparticles are found with some agglomerations which are typical for porous surface with high surface area. High surface area to volume ratio of nanoparticles provides a very high surface energy. For reducing surface energy via strong magnetic dipole-dipole attractions among the particles they tend to agglomerate [18]. So the aggregations may be because of the magnetic interfaces amongst the iron oxide nanoparticles or the grain growth at higher calcination temperature for the minimization of Gibbs free energy resulting from the reduction of extended surface area of nanoparticle [26]. The average particle size has been calculated by using Image J software which are listed in Table 3. It is clear that the particle size increases with higher calcination temperature and time (800 °C, 6 h) which also matched from the data obtained from XRD. Whereas, the average particle sizes are nearly same for samples calcined at 600 & 700°C.

3.4. Elemental analysis by EDS

Fig. 5(a–e) exhibits the purity of the calcined α-Fe_2O_3, in which only one peak for oxygen (O) and three peaks of iron (Fe) in all the synthesized hematite nanoparticles. Whereas an additional signal observed in the sample calcined at 700 °C, 4 h. The EDS spectra of α-Fe_2O_3 nanoparticles calcined at different temperature and time are shown in Table 4. The atomic ratio of Fe/O is very close (0.63) to stoichiometric value of 0.66 in case of the sample calcined at 700 °C, 3 h.

3.5. Chemical state by XPS

The chemical state of Fe and O atoms and the surface composition of hematite nanoparticles were studied by XPS. Fig. 6 shows the high resolution XPS spectra of Fe 2p. Fig. 6(a) shows the survey spectrum data of α-Fe_2O_3 nanoparticles calcined at 600 °C, 4 h and 700 °C, 4 h respectively and it was revealed that the nanoparticles were primarily composed of iron (Fe) and oxygen (O). The findings are in tandem with the EDS result as discussed earlier. Fig. 6(b) and (c) show the more details about Fe 2p and the both spectrum showed Fe^{3+} 2p $_{3/2}$ and Fe^{3+} 2p $_{1/2}$ the peaks with satellite feature. In Fig. 6(b) and (c) the doublet of Fe^{3+} 2p $_{3/2}$ and Fe^{3+} 2p $_{1/2}$ having the binding energy 711.02 eV, 710.90 eV and 724.38 eV, 724.22 eV and a satellite peak observed at 718.93 eV, 718.89 corresponds to Fe^{3+} 2p $_{3/2}$. These values are in good agreement the previous reports which indicating the synthesized nanoparticles were pure hematite [25,26,41,42].

Table 6
Z-average hydrodynamic diameter $\overline{D}_h$ and polydispersity index (PDI) of α-Fe_2O_3 nanoparticles calcined at different temperatures and times.

Calcination Temperature (°C) & Time (h)	$\overline{D}_h$ nm	PDI
600, 3	202	0.271
600, 4	207	0.283
700, 3	446	0.338
700, 4	342	0.385
800, 6	514	0.251

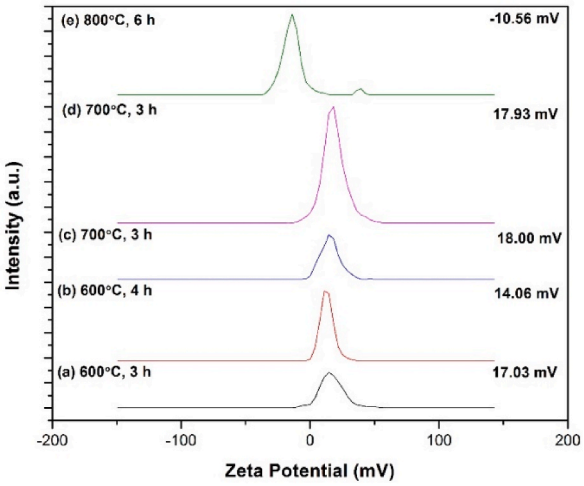

Fig. 8. Zeta potential value of α-Fe_2O_3 nanoparticles calcined at different temperature and time.

3.6. BET analysis

The surface area of the nanoparticles was measured by low-temperature nitrogen adsorption (N2-BET) tests. According to IUPAC (International Union of Pure and Applied Chemistry) classification, the types of pores and isotherms were defined. Porous material is signified as micropores (<2 nm in diameter), mesopores (2–50 nm in diameter) and macropores (>50 nm in diameter). The specific surface area, total pore volume and average pore diameter of the nanoparticles calcined at 600 °C, 4 h and 700 °C, 4 h are summarizes in Table 5. The results (Table 5) indicated that the BET specific surface area for hematite nanoparticles (α-Fe_2O_3) were found as 33.55 m^2/g and 12.74 m^2/g much higher than the surface area possessed by commercial α-Fe_2O_3 nanoparticles (6 m^2/g) [25,26]. The high surface area (calcined at 600 °C, 4 h) obtained in the study was also supported by the SEM image result. The surface area largely affects the pore diameter and pore volume of the nanoparticles. Surface area is associated to pore diameter in which the surface area is relatively large the pore diameter is small. From the pore volume analysis, the pore volumes of the hematite nanoparticles calcined at 600 °C, 4 h and 700 °C were obtained as 0.1028 cm^3/g and 0.0260 cm^3/g and the average pore diameter size were 12.26 nm and 8.16 nm respectively which supported the mesoporous structure of the pores [25,26].

3.7. Particle size analysis by dynamic light scattering measurements (DLS)

Particle size distribution of hematite nanoparticles are shown in Fig. 7. The Z-average apparent hydrodynamic diameter $\overline{D}_h$ was calculated from the Z-average translation diffusion coefficient $\overline{D}$ through the stokes-Einstein equation (Eqn. (3)) [6]:

$$\overline{D}_h = \frac{k_B T}{3\pi\eta\overline{D}} (2) \tag{3}$$

where k_B is the Boltzmann constant and η is the solvent viscosity at temperature T. The Z-average apparent hydrodynamic diameter $\overline{D}_h$ and polydispersity index (PDI) are recorded in Table 6.

It is clearly demonstrated from Table 6 that the nano particles are poly dispersed with an effective (cumulate) diameter of $\overline{D}_h = 202$ and 207 nm for the samples calcined at 600 °C, 3 h and 600 °C, 4 h respectively. As the calcination temperature increases, the particle size increases but the $\overline{D}_h$ value is lower (342 nm) for higher calcined time (4 h) than the $\overline{D}_h$ value (446 nm) of lower calcined time (3 h). This data also matched with all the data obtained by different technique (XRD, SEM). DLS gives the hydrodynamic diameter and measures the time dependent fluctuation in the intensity of scattered light due to Brownian motion of the particles, so the results of DLS

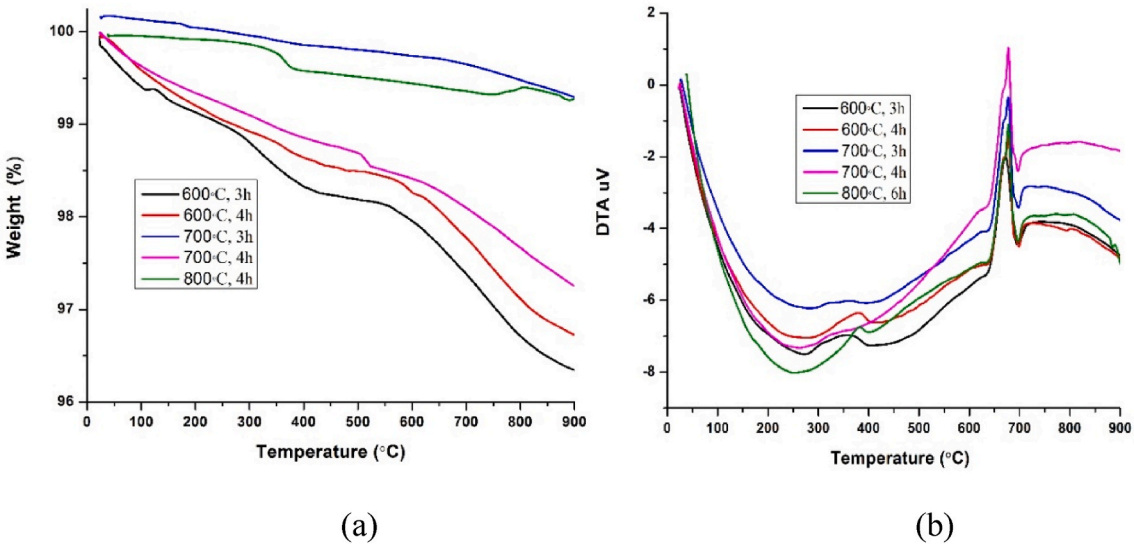

Fig. 9. (a) TG and (b) DTA curve of α-Fe_2O_3nanoparticles calcined at different temperatures and times.

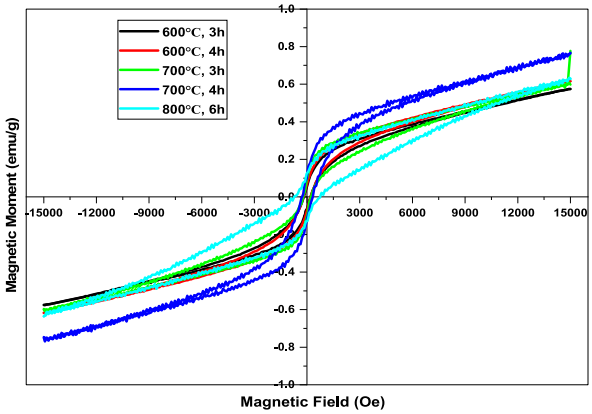

Fig. 10. Hysteresis loop of prepared α-Fe_2O_3 nanoparticles calcined at distinct temperatures and times.

are not in agreement with SEM and XRD data [6] and the hydrodynamic diameter is much higher than the calculated XRD and SEM values reported in Tables 2 and 3 [18].

3.8. Zeta potential analysis

For the measurement of zeta potential, 10 mg of each calcined hematite nano particles were taken in 100 ml deionized water and then sonicated for 30 min. The dispersed solution was ready for measuring zeta potential. Fig. 8 show the zeta potential values of calcined hematite (α-Fe_2O_3) nanoparticles.

The zeta potential value of hematite (α-Fe2O3) nanoparticles calcined at different temperatures and times (a) - (e) are 17.03 mV, 14.06 mV, 18.00 mV, 17.93 mV and −10.56 mV respectively. Hematite suspension was stable at pH less than 6.0 or above 10.0 [43]. The nanoparticles become unstable when nanoparticles are dispersed in distilled water (pH = 7) and accumulate owing to its high surface area and electrostatic forces between the particles [44]. Particles having zeta potential value higher than +30 mV or lower than –30 mV are regarded stable condition. A stable system could form when the repulsive force exceeds the attractive force [45]. The particles in a suspension having a large negative or positive zeta potential value will tend to counteract each other and there have no tendency for the particles to come together. According to the DLVO theory, a system can be regarded as stable if the electrostatic repulsion dominates the attractive van der Waals force [46]. The particles having low zeta potential value of –10.56 mV for the sample calcined at 800 °C, 6 h indicates that the insufficient repulsion to prevent the particles coming together and flocculating. The effective zeta potential of small particles is greater than that of larger particles as well as small diameter particles are easily affected by the random movement of fluid flow [47]. This data also supported the particle size data obtained from SEM and DLS.

Table 7
Magnetic susceptibility data of α-Fe_2O_3 nanoparticles calcined at different temperatures and times.

Calcination Temperature (°C) & Time (h)	Coercivity (Oe) Hc	Remnant mass magnetization (emu/g) Mr	Saturation mass magnetization (emu/g) Ms
600, 3	0.0119	0.0593	0.5620
600, 4	0.0174	0.0694	0.6029
700, 3	0.0170	0.0987	0.5910
700, 4	0.0280	0.1159	0.7451
800, 6	0.0245	0.1277	0.6143

3.9. Thermal analysis

Fig. 9 shows the thermal analysis of α-Fe_2O_3 nanoparticles calcined at different temperature and time. The thermo-gravimetric analysis showed no significant change in weight loss increase in temperature for the calcined samples. The weight loss percentage is near about 0.6–4%. The instrument was not stable at the beginning of the test (0–30 min), the TG value was a little more than 100% [48] for the sample calcined at 700 °C, 3 h.TGA curve shows, there are two distinct mass loss steps in the temperature ranges 25 °C–400 °C and 550 °C–990 °C respectively for all the calcined sample. The first mass loss is due to the evaporation of surface adsorbed water as well as chemically adsorbed water [22], volatilization and combustion products of organic species [3] and the second one is decomposition of prepared samples which are also observed in DTA curve in the temperature range 635 °C–700 °C.

3.10. Magnetic studies

Fig. 10 shows the magnetic hysteresis loop of prepared nanomaterials which characterize the dependence of magnetization on the applied magnetic field. The hysteresis loop indicates that all these hematite nanoparticles have ferromagnetic behavior, and the sample synthesized at 700 °C for 4 h has the maximum saturation magnetization (Ms) 0.74512 emu/g at maximum applied magnetic field (Mmax) 14500 Oe [49] which is greater than the commercially available hematite (0.6 emu/g) [25,26]. All the three samples possess wide open M − H loops with the remnant magnetization (Mr) and the coercivity (Hc). The coercivity has been affected by the size and shape anisotropy of the synthesized particles [50]. Coercivity (Hc), remnant magnetization (Mr) and saturation magnetization (Ms) are listed in Table 7. It is clearly seen that the sample of 600 °C & 3 h calcination temperature and time, exhibited an extremely small hysteresis loop and low coercivity compared to other samples which persuades by various factors like size and shape of particles, crystallinity, defects in crystal, etc [51].

4. Conclusion

In the present study we have been synthesized hematite (α-Fe_2O_3) nanoparticles successfully from waste condensed milk containers which contain a remarkable amount (93.3%) of iron. XRD measurements of the samples calcined at different temperature and time confirm that the prepared nanoparticles consist only hematite phase, also supported by FTIR results. The SEM analysis of the samples illustrate that the particles are agglomerated and irregular spherical shape with average particle size range from 45 to 149 nm. Particle size and distribution obtained from both SEM and DLS result are in good agreement with each other. The elemental Fe and O were noticed in the EDS analysis as well as the surface chemistry and chemical state of Fe 2p and O1s were also measured by XPS. In addition, the EDS, XRD, and XPS analyses revealed the purity of the hematite nanoparticles. High surface area (33.55 m^2/g) of the nanoparticles calcined at 600 °C, 4 h with mesoporous structure was performed by BET. The stability of the samples was examined by the zeta potential value and it is clear that the samples are unstable in neutral pH. Maximum saturation magnetization (Ms) (0.74512emu/g) was achieved for the sample calcined at 700 °C, 4 h. The weight loss percentage of the samples was measured by thermo-gravimetric analysis. The present study carried out on five synthetic samples calcined at distinct temperature and time shows that they composed of pure hematite phase with nearly same morphology and different particle size.

Acknowledgements

The work has been carried out in Ceramic Raw materials and Ceramic Materials Testing Division, Institute of Glass and Ceramic Research and Testing (IGCRT), Bangladesh Council of Scientific and Industrial Research (BCSIR), Dhaka, Bangladesh. The authors are grateful for the financial support from Bangladesh Council of Scientific and Industrial Research (BCSIR). The authors would like to thank Pilot Plant and Process Development center, PP&PDC, BCSIR; Central Analytical and Research Facilities, CARF, BCSIR; Institute of Fuel Research and Development, IFRD, BCSIR; Glass Research Division, IGCRT, BCSIR, Dhaka for providing technical supports.

References

[1] D.M.S.N. Dissanayake, M.M.M.G. Mantilaka, T.C. Palihawadana, G.T.D. Chandrakumara, R.T. De Silva, H.M.T.G.A. Pitawala, K.M. Nalin De Silva, G.A. J. Amaratunga, Facile and low-cost synthesis of pure hematite (α-Fe2O3) nanoparticles from naturally occurring laterites and their superior adsorption capability towards acid-dyes, RSC Adv 9 (2019) 21249–21257, https://doi.org/10.1039/c9ra03756j.
[2] L.Y. Novoselova, Hematite nanoparticle clusters with remarkably high magnetization synthesized from water-treatment waste by one-step "sharp high-temperature dehydration, RSC Adv 7 (2017) 51298–51302, https://doi.org/10.1039/c7ra09062e.

[3] S.C.K.G. Bagheri, Generation of hematite nanoparticles via sol-gel method, Res. J. Chem. Sci. 3 (2013) 62–68. http://www.isca.in/rjcs/Archives/vol3/i7/9.ISCA-RJCS-2013-097.pdf.

[4] H. Mansour, K. Omri, S. Ammar, Structural, optical and magnetic properties of cobalt doped hematite nanoparticles, Chem. Phys. 525 (2019), 110400, https://doi.org/10.1016/j.chemphys.2019.110400.

[5] N.Y. Dzade, A. Roldan, N.H. de Leeuw, A density functional theory study of the adsorption of benzene on hematite (α-Fe2O3) surfaces, Minerals 4 (2014) 89–115, https://doi.org/10.3390/min4010089.

[6] C. Colombo, G. Palumbo, A. Ceglie, R. Angelico, Characterization of synthetic hematite (α-Fe 2O 3) nanoparticles using a multi-technique approach, J. Colloid Interface Sci. 374 (2012) 118–126, https://doi.org/10.1016/j.jcis.2012.02.003.

[7] G.L. Lima, R.W.L. Oliveira, R.M. de Jesus Neto, A.M.d.S. Gomes, R.A. Fiuza Junior, H.M.C. Andrade, A.J.S. Mascarenhas, Single step synthesis of magnetic materials derived from biomass residues, Waste and Biomass Valorization 12 (2021) 1039–1050, https://doi.org/10.1007/s12649-020-01003-7.

[8] Q. Dong, D. Wang, J. Yao, N. Kumada, N. Kinomura, T. Takei, Y. Yonesaki, Q. Cai, Synthesis of hematite particles with various shapes by a simple hydrothermal reaction, J. Ceram. Soc. Japan. 117 (2009) 245–248, https://doi.org/10.2109/jcersj2.117.245.

[9] J.W. Park, J.C. Ahn, H. Song, K. Park, H. Shin, J.S. Ahn, Reduction characteristics of oily hot rolling mill sludge by direct reduced iron method, Resour. Conserv. Recycl. 34 (2002) 129–140, https://doi.org/10.1016/S0921-3449(01)00098-2.

[10] M. Tadic, M. Panjan, B.V. Tadic, J. Lazovic, V. Damnjanovic, M. Kopani, L. Kopanja, Magnetic properties of hematite (α - Fe2O3) nanoparticles synthesized by sol-gel synthesis method: the influence of particle size and particle size distribution, J. Electr. Eng. 70 (2019) 71–76, https://doi.org/10.2478/jee-2019-0044.

[11] L.M. Khoiroh, M.N. Al-Chabib, A. Prasetyo, Synthesis and characterization of hematite (α-Fe2O3) from lathe waste using co-precipitation -calcination method, IOP Conf. Ser. Mater. Sci. Eng. 578 (2019), https://doi.org/10.1088/1757-899X/578/1/012004.

[12] E. Esmaeili, M. Salavati-Niasari, F. Mohandes, F. Davar, H. Seyghalkar, Modified single-phase hematite nanoparticles via a facile approach for large-scale synthesis, Chem. Eng. J. 170 (2011) 278–285, https://doi.org/10.1016/j.cej.2011.03.010.

[13] M. Zhu, Y. Wang, D. Meng, X. Qin, G. Diao, Hydrothermal synthesis of hematite nanoparticles and their electrochemical properties, J. Phys. Chem. C 116 (2012) 16276–16285, https://doi.org/10.1021/jp304041m.

[14] S. Naz, M. Islam, S. Tabassum, N.F. Fernandes, E.J. Carcache de Blanco, M. Zia, Green synthesis of hematite (α-Fe 2 O 3) nanoparticles using Rhus punjabensis extract and their biomedical prospect in pathogenic diseases and cancer, J. Mol. Struct. 1185 (2019) 1–7, https://doi.org/10.1016/j.molstruc.2019.02.088.

[15] S. Xu, A.H. Habib, S.H. Gee, Y.K. Hong, M.E. McHenry, Spin orientation, structure, morphology, and magnetic properties of hematite nanoparticles, J. Appl. Phys. 117 (2015), https://doi.org/10.1063/1.4914059.

[16] Y. Xu, S. Yang, G. Zhang, Y. Sun, D. Gao, Y. Sun, Uniform hematite α-Fe2O3 nanoparticles: morphology, size-controlled hydrothermal synthesis and formation mechanism, Mater. Lett. 65 (2011) 1911–1914, https://doi.org/10.1016/j.matlet.2011.03.085.

[17] V. Kumar, S. Chahal, D. Singh, A. Kumar, P. Kumar, K. Asokan, Annealing effect on the structural and dielectric properties of hematite nanoparticles, AIP Conf. Proc. 1953 (2018), https://doi.org/10.1063/1.5032580.

[18] D.E. Fouad, C. Zhang, H. El-Didamony, L. Yingnan, T.D. Mekuria, A.H. Shah, Improved size, morphology and crystallinity of hematite (α-Fe2O3) nanoparticles synthesized via the precipitation route using ferric sulfate precursor, Results Phys. 12 (2019) 1253–1261, https://doi.org/10.1016/j.rinp.2019.01.005.

[19] N.D. Cuong, T.T. Hoa, D.Q. Khieu, N.D. Hoa, N. Van Hieu, Gas sensor based on nanoporous hematite nanoparticles: effect of synthesis pathways on morphology and gas sensing properties, Curr. Appl. Phys. 12 (2012) 1355–1360, https://doi.org/10.1016/j.cap.2012.03.026.

[20] J.H. Bang, K.S. Suslick, 1211, J. Am. Chem. Soc. 129 (2007) 2242–2243.

[21] H.M. Asoufi, T.M. Al-Antary, A.M. Awwad, Green route for synthesis hematite (α-Fe2O3) nanoparticles: toxicity effect on the green peach aphid, Myzus persicae (Sulzer), Environ. Nanotechnol. Monit. Manag. 9 (2018) 107–111, https://doi.org/10.1016/j.enmm.2018.01.004.

[22] E. Darezereshki, One-step synthesis of hematite (α-Fe2O3) nano-particles by direct thermal-decomposition of maghemite, Mater. Lett. 65 (2011) 642–645, https://doi.org/10.1016/j.matlet.2010.11.030.

[23] D. Hassan, A.T. Khalil, J. Saleem, A. Diallo, S. Khamlich, Z.K. Shinwari, M. Maaza, Biosynthesis of pure hematite phase magnetic iron oxide nanoparticles using floral extracts of Callistemon viminalis (bottlebrush): their physical properties and novel biological applications, Artif. Cells, Nanomedicine Biotechnol 46 (2018) 693–707, https://doi.org/10.1080/21691401.2018.1434534.

[24] K. de Fátima Ulbrich, C.E.M. de Campos, Obtaining of hematite from industrial steel waste using dry-milling and high temperature, Clean. Eng. Technol. 5 (2021), https://doi.org/10.1016/j.clet.2021.100327.

[25] P. Prabhu, M. Rao, G. Murugesan, M.K. Narasimhan, T. Varadavenkatesan, R. Vinayagam, N.T. Lan Chi, A. Pugazhendhi, R. Selvaraj, Synthesis, characterization and anticancer activity of the green-synthesized hematite nanoparticles, Environ. Res. 214 (2022), 113864, https://doi.org/10.1016/j.envres.2022.113864.

[26] R. Vinayagam, Y. Patnaik, P. Brijesh, D. Prabhu, M. Quadras, S. Pai, M.K. Narasimhan, K. Kaviyarasu, T. Varadavenkatesan, R. Selvaraj, Superparamagnetic hematite spheroids synthesis, characterization, and catalytic activity, Chemosphere 294 (2022), 133730, https://doi.org/10.1016/j.chemosphere.2022.133730.

[27] F. Magdoff, The Depletion of the World's Natural Resources Is Population the Problem?, 2011, pp. 13–28.

[28] N. Rotzer, M. Schmidt, Decreasing metal ore grades-Is the fear of resource depletion justified? Resources 7 (2018) https://doi.org/10.3390/resources7040088.

[29] WasteWise, The economic benefits of recycling and waste reduction – WasteWise case studies from the private and public sectors | 2, New Jersey WasteWise Bus. Netw. (2013) 1–12.

[30] R. Bott, Environmental benefits of recycling, Wrap (2014) 1–5.

[31] O. Benchiheub, S. Mechachti, S. Serrai, M.G. Khalifa, Elaboration of iron powder from mill scale, J. Mater. Environ. Sci. 1 (2010) 267–276.

[32] B. Das, S. Prakash, P.S.R. Reddy, V.N. Misra, An overview of utilization of slag and sludge from steel industries, Resour. Conserv. Recycl. 50 (2007) 40–57, https://doi.org/10.1016/j.resconrec.2006.05.008.

[33] M.A. Legodi, D. de Waal, The preparation of magnetite, goethite, hematite and maghemite of pigment quality from mill scale iron waste, Dyes Pigments 74 (2007) 161–168, https://doi.org/10.1016/j.dyepig.2006.01.038.

[34] H.M. Veit, T.R. Diehl, A.P. Salami, J.S. Rodrigues, A.M. Bernardes, J.A.S. Tenorio, Utilization of magnetic and electrostatic separation in the recycling of printed circuit boards scrap, Waste Manag 25 (2005) 67–74, https://doi.org/10.1016/j.wasman.2004.09.009.

[35] B. Liu, S. Zhang, D. Pan, C. Chang, Synthesis and characterization of micaceous iron oxide pigment from oily cold rolling mill sludge, Procedia Environ. Sci. 31 (2016) 653–661, https://doi.org/10.1016/j.proenv.2016.02.121.

[36] L. Rahman, S. Bhattacharjee, S. Islam, F. Zahan, B. Biswas, N. Sharmin, A study on the preparation and characterization of maghemite (γ-Fe2O3) particles from iron-containing waste materials, J. Asian Ceram. Soc. 8 (2020) 1083–1094, https://doi.org/10.1080/21870764.2020.1812838.

[37] S.R. Prim, M.V. Folgueras, M.A. de Lima, D. Hotza, Synthesis and characterization of hematite pigment obtained from a steel waste industry, J. Hazard Mater. 192 (2011) 1307–1313, https://doi.org/10.1016/j.jhazmat.2011.06.034.

[38] M. Quddus, M. Rahman, J. Khanam, B. Biswas, N. Sharmin, S. Ahmed, A. Neger, Synthesis and characterization of pigment grade red iron oxide from mill scale, Int. Res. J. Pure Appl. Chem. 16 (2018) 1–9, https://doi.org/10.9734/irjpac/2018/42935.

[39] B. Biswas, J. Khanam, L. Rahman, S. Rahman, N. Sharmin, S. Ahmed, T. Neger, Fabrication of ferrous sulfate from waste like condensed milk can and its characterization fabrication of ferrous sulfate from waste like condensed milk containing can and its characterization, Technol. Sci. Am. Sci. Res. J. Eng. 42 (2018) 157–165. http://asrjetsjournal.org/.

[40] T. Gong, Y. Tang, Preparation of multifunctional nanocomposites Fe3O4@SiO2-EDTA and its adsorption of heavy metal ions in water solution, Water Sci. Technol. 81 (2020) 170–177, https://doi.org/10.2166/wst.2020.099.

[41] M.I.U. Hoque, Y. Yamauchi, R. Naidu, R. Holze, R. Saidur, Q. Qu, M.M. Rahman, N.L. Torad, M.S.A. Hossain, M. Kim, J. Kim, S.H.A. Ahmad, A.U. Rehman, M.S. H. Firoz, U. Luba, S. Chowdhury, A.N. Chowdhury, A facile synthesis of hematite nanorods from rice starch and their application to Pb(II) ions removal, ChemistrySelect 4 (2019) 3730–3736, https://doi.org/10.1002/slct.201802462.

[42] M. Fondell, M. Gorgoi, M. Boman, A. Lindblad, Surface modification of iron oxides by ion bombardment – comparing depth profiling by HAXPES and Ar ion sputtering, J. Electron. Spectrosc. Relat. Phenom. 224 (2018) 23–26, https://doi.org/10.1016/j.elspec.2017.09.008.

[43] C.Y. Xu, R.K. Xu, J.Y. Li, K.Y. Deng, Phosphate-induced aggregation kinetics of hematite and goethite nanoparticles, J. Soils Sediments 17 (2017) 352–363, https://doi.org/10.1007/s11368-016-1550-y.
[44] P.S. Sundara Selvam, S. Govindan, B. Perumal, V. Kandan, Screening of in vitro antibacterial property of hematite (α-Fe2O3) nanoparticles: a green approach, Iran, J. Sci. Technol. Trans. A Sci. 45 (2021) 177–187, https://doi.org/10.1007/s40995-020-00995-0.
[45] M. Larsson, A. Hill, J. Duffy, Suspension stability: why particle size, zeta potential and rheology are important product technical specialists rheometry products malvern instruments limited, Annu. Trans. Nord. Rheol. Soc. (2012) 1999.
[46] C. Freitas, R.H. Muller, Effect of light and temperature on zeta potential and physical stability in solid lipid nanoparticle (SLN®) dispersions, Int. J. Pharm. 168 (1998) 221–229, https://doi.org/10.1016/S0378-5173(98)00092-1.
[47] Y. Nakatuka, H. Yoshida, K. Fukui, M. Matuzawa, The effect of particle size distribution on effective zeta-potential by use of the sedimentation method, Adv. Powder Technol. 26 (2015) 650–656, https://doi.org/10.1016/j.apt.2015.01.017.
[48] Y. Qu, Y. Yang, Z. Zou, C. Zeilstra, K. Meijer, R. Boom, Thermal decomposition behaviour of fine iron ore particles, ISIJ Int. 54 (2014) 2196–2205, https://doi.org/10.2355/isijinternational.54.2196.
[49] M.M. Rafi, K.S.Z. Ahmed, K.P. Nazeer, D. Siva Kumar, M. Thamilselvan, Synthesis, characterization and magnetic properties of hematite (α-Fe2O3) nanoparticles on polysaccharide templates and their antibacterial activity, Appl. Nanosci. 5 (2015) 515–520, https://doi.org/10.1007/s13204-014-0344-z.
[50] M. Gaidhane, Nanocrystalline α-Fe2O3: a superparamagnetic material for w-LED application and waste water treatment, Res. Sq. 1 (2021) 1–21.
[51] M. Ahmadzadeh, C. Romero, J. McCloy, Magnetic analysis of commercial hematite, magnetite, and their mixtures, AIP Adv. 8 (2018), https://doi.org/10.1063/1.5006474.